Respiratory rate detection algorithm based on RGB-D camera: theoretical background and experimental results

Flavia Benetazzo, Alessandro Freddi, Andrea Monteriù, Sauro Longhi

Dipartimento di Ingegneria dell'Informazione, Università Politecnica delle Marche, Ancona, Italy
E-mail: f.benetazzo@univpm.it

Published in Healthcare Technology Letters; Received on 22nd April 2014; Revised on 5th August 2014; Accepted on 2nd September 2014

Both the theoretical background and the experimental results of an algorithm developed to perform human respiratory rate measurements without any physical contact are presented. Based on depth image sensing techniques, the respiratory rate is derived by measuring morphological changes of the chest wall. The algorithm identifies the human chest, computes its distance from the camera and compares this value with the instantaneous distance, discerning if it is due to the respiratory act or due to a limited movement of the person being monitored. To experimentally validate the proposed algorithm, the respiratory rate measurements coming from a spirometer were taken as a benchmark and compared with those estimated by the algorithm. Five tests were performed, with five different persons sat in front of the camera. The first test aimed to choose the suitable sampling frequency. The second test was conducted to compare the performances of the proposed system with respect to the gold standard in ideal conditions of light, orientation and clothing. The third, fourth and fifth tests evaluated the algorithm performances under different operating conditions. The experimental results showed that the system can correctly measure the respiratory rate, and it is a viable alternative to monitor the respiratory activity of a person without using invasive sensors.

1. Introduction: This Letter deals with a respiratory rate measurement algorithm that uses a red green blue-depth (RGB-D) camera. Breathing is a fundamental physiological task in living organisms, and there are many respiratory diseases that require attentive care and respiratory training. For this reason, it is particularly important to monitor the respiratory activity of a human being. Among invasive methods, it is possible to cite the spirometer, pneumotachography, respiratory inductance plethysmography [1, 2] or thermistor [3]. There are studies trying to obtain breath rate activity from pulse oximiters [4, 5]; however, oximetry alone is of limited value in the investigation of the user breath and it is not common. They all are state-of-the-art devices which can be adopted to measure the respiratory activity; however, they require a direct contact with the person to be monitored, and may interfere with the natural respiration activity (e.g. physical limitation, stress, unease, etc.). To overcome this limitation, non-invasive devices are required instead. In the literature, several systems have been investigated: CCD camera [6], structured light plethysmography [7], slit light projection pattern [8] or ultra-wideband sensors [9]. The use of RGB-D cameras for the detection of breathing is quite a recent technique and is described in only a few papers in the literature such as [10–16]. In [10], the authors describe two approaches (respiratory rate and leg jiggling measurement) for unobtrusively sensing subtle non-verbal behaviours using the RGB-D camera. A vision-based method to estimate the respiration rate of subjects from their chest movements using principal component analysis and autoregressive spectral analysis is presented in [11]. In [12], a system is developed to measure human chest wall motion for respiratory volume estimation without any physical contact, while in [13], a depth analysis technique was developed to monitor the users' sleep conditions without any physical contact. Reference [14] proposes a Kinect-based respiratory monitoring system that overcomes the limitation of Kinect's depth resolution and achieves real-time respiratory tracking. In [15] the authors propose to use an active-stereo-based depth sensing system for forced flow-volume loop measurements and for semi-automatic and automatic assessment of abnormal breathing patterns. In [16], it is possible to see how a vision-based method can be used for recovering the cardiac pulse rate from recordings of the human face.

In this Letter, the RGB-D camera is used as a sensor, which provides the needed information to be processed by the proposed algorithm and to measure the respiratory rate of a sitting person in an indoor environment. The innovative contribution of the present work is regarding the development of an algorithm that automatically identifies the respiratory rate with a low-cost system, and thus can be used without overly restrictive constraints. Moreover, unlike the papers mentioned previously, the algorithm has been experimentally tested both in nominal and non-nominal conditions, in order to verify its robustness with respect to common disturbances that can affect such systems, that is, variation in environmental light, user orientation and clothing. Video 1 shows an experimental demonstration of the system.

The Letter is organised as follows: Section 2 describes the hardware and software adopted for developing the low-cost system. Section 3 details the problem of detecting a person and finding his/her respiratory rate through the use of the RGB-D camera. Section 4 shows the experimental results in different operating conditions. Finally, Section 5 summarises the key points of the paper and provides an overview of the future developments of the respiratory rate measurement algorithm.

2. System configuration: The proposed respiratory rate detection algorithm exploits low-cost hardware and an open source software.

2.1. Hardware: A RGB-D camera is a vision sensor, which can also measure the distance of objects within its field of view. A RGB-D camera is used for the identification of persons and objects, even if the background and the person or the object have the same colour. RGB-D cameras can recognise overlapped objects by calculating the distance for each of them.

RGB-D Structured Light (SL) cameras are sensing systems that capture RGB images along with per-pixel depth information. In detail, RGB-D SL cameras project a known pattern onto the scene or subject of interest, and the distortion in the project pattern encodes the depth information of the scene or object. The principle of SL cameras is that, given a specific angle between emitter and sensor, the depth can be recovered from triangulation. An SL camera is composed of an infrared (IR) projector, a diffraction grating and a standard complementary metal oxide

semiconductor (CMOS) detector with a band-pass filter centred at the IR light wavelength. The diffraction grating is a computer-generated hologram, which produces a specific periodic structure of IR light when the laser shines through it. The projected image does not change in time. The IR CMOS sensor detects this pattern projected onto the room and scene, and generates the corresponding depth image. Compared with cameras based on time of flight (TOF) technology, SL cameras have a shorter range and images appear to be noisier and less accurate. Post-processing algorithms can, however, take care of these issues. Moreover, SL cameras are much cheaper than TOF cameras. Further information on SL cameras can be found in [17].

SL sensors are proven to be effective for breath rate measurement as well [10–13]: the sensors' resolution is usually adequate to sense small movements like those performed by the thorax during the respiratory phase [18]. An innovative RGB-D SL camera, namely the Kinect camera, has been adopted to develop the proposed respiratory rate detection algorithm.

2.2. Software: Open Natural Interaction (OpenNI) is used to implement further functionalities of the vision sensor. OpenNI is a multi-language and multi-platform framework that defines the application programming interface (API) for writing applications that use natural interaction, that is, interfaces that do not require remote controls, but allow people to interact with a machine through gestures and words typical of human–human interactions. This API has been chosen because it incorporates algorithms for background suppression and identification of people motion, without causing a slowdown in the video.

3. Respiratory rate detection: To measure the human respiratory rate, the person has to be identified. This operation is called calibration. The calibration algorithm recognises different parts of the person's body, associating a point (joint) to each of them. The calibration operation is required by the vision sensor to find the person in its field of view and is performed by using the functionalities already available within the OpenNI library. After this procedure, the proposed respiratory rate detection algorithm starts. The respiratory rate detection algorithm counts the number of breaths per minute of a person. Using the depth information provided by the camera, the algorithm identifies the person's chest and calculates the mean value of the depth of the chest at each time

$$\bar{D}(k) = \frac{\sum_{i=1}^{N} D_i(k)}{N} \tag{1}$$

where $D_i(k)$ is the information of the depth at the ith point associated to the chest at the sampling instant k, and N is the number of points of the chest. The mean value $\bar{D}(k)$ is calculated using data sampled at the frequency of $1/T_c = 7$ Hz, where T_c is the sampling time. A sampling frequency of 7 Hz was chosen because this frequency allows one to obtain the most accurate respiratory rate, as detailed in Section 4.1. The initial position of the chest of the monitored person is used as the reference value. The subsequent measurements are used to identify the number of breaths.

The algorithm calculates the weighted average of the mean values of the depth. This weighted average WA(k) is calculated over a sliding window of four samples with the following formula

$$\mathrm{WA}(k) = \sum_{i=0}^{3} w_{k-i}\bar{D}(k-i) \tag{2}$$

where $\bar{D}$ is calculated according to (1) and w_{k-i} (where $w_{k-i} \leq 1$, $\forall i \leq 3$) is the weight associated to the mean value $D(k-i)$. The choice of the sliding window size (four samples) is a trade-off between noise rejection and loss of depth information caused by averaging over large window size. The weights are $w_k = 1$, $w_{k-1} = 0.7$, $w_{k-2} = 0.4$ and $w_{k-3} = 0.1$, in order to give more importance to the last samples. After calculating the weighted average, the algorithm calculates the derivative of the weighted average as

$$\mathrm{dWA}(k) = \frac{\mathrm{WA}(k) - \mathrm{WA}(k-1)}{T_c} \tag{3}$$

The proposed analysis of the derivative allows one to identify the maxima and the minima of the average value, and to eliminate irregularities in breathing. In fact, in case of irregularities, the analysis of the weighted average is not sufficient to calculate the number of breaths. The algorithm analyses the derivative and counts the number of times that it becomes positive to calculate the respiratory rate. To do this, the algorithm automatically analyses the sign of the derivative, detects when it changes and checks if that sign is kept for at least three samples. In detail, if the sign changes from negative into positive, a new breath is detected. If the sign changes from positive into negative, the breath passes from the inhalation phase to the exhalation phase. The algorithm checks that the change of the sign persists for at least three samples in order to avoid disturbances overlaid on the signal which may cause an incorrect count. In this way, the algorithm automatically counts the number of breaths.

It is possible to extract further information from the weighted average and the derivative:

Time of exhalation, $\Delta \mathrm{TE}_i = \mathrm{TE}_i - \mathrm{TI}_{i-1}$
Time of inhalation, $\Delta \mathrm{TI}_i = \mathrm{TI}_i - \mathrm{TE}_{i-1}$
Depth of exhalation, $\Delta \mathrm{DE}_i = \mathrm{WA}(\mathrm{TE}_i/T_c) - \mathrm{WA}(\mathrm{TI}_{i-1}/T_c)$
Depth of inhalation, $\Delta \mathrm{DI}_i = \mathrm{WA}(\mathrm{TI}_i/T_c) - \mathrm{WA}(\mathrm{TE}_{i-1}/T_c)$

where TE_i is the instant of time in which the exhalation of the ith breath ends, TI_i is the instant of time in which the inhalation of the ith breath ends, WA($\cdot$) is the average value of the mean values of the depth of the chest at the sampling instant in which the exhalation or the inhalation of the considered breath ends. If the person moves during the measurement, then the algorithm records the information, recalculates the position of the chest and uses it as the new reference value. Once the measurement ends, if the person moved during the acquisition, the algorithm reconstructs the mean value of the depth of the chest $\left(\bar{D}(\cdot)\right)$. At the instant in which the user started to move, the mean value of the depth of the chest $\left(\bar{D}(\cdot)\right)$ undergoes a shift. In order to properly calculate the number of breaths, the algorithm sums the mean value of the signal $\bar{D}(\cdot)$ before the shift to the value of the signal $\bar{D}(\cdot)$ after the movement.

The algorithm introduced above can be resumed by the following steps:

1. Detection of torso and shoulders: These are the points that allow finding the chest of the user.
2. Definition of the region of interest (ROI): The ROI is the chest of the person, which is within the region delimited by the shoulder and the torso, as shown in Fig. 1.
3. Depth measurements: The depths of all points inside the box are measured.
4. Calculation of the mean value of the depth: Calculation of the mean value of the depth of the points inside the ROI is performed. If the person is moving, the algorithm recalculates the torso and shoulders coordinates (step 1). When the online part of the algorithm (measurement) ends, then the mean values of the z coordinates are evaluated offline to find the respiratory rate, see Fig. 2.
5. Calculation of the weighted average on a sliding window of four samples: If the user moves during the acquisition, the mean value of the depth of the chest (calculated at step 4) is reconstructed by summing the mean value of the signal before the movement to

doi: 10.1049/htl.2014.0063

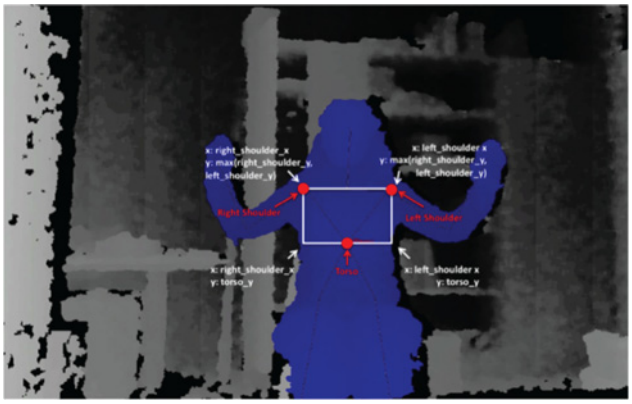

Figure 1 *Region of interest*
The white arrows indicate the vertices of the box and their coordinates
The red arrows indicate the torso and shoulders joints found in step 1

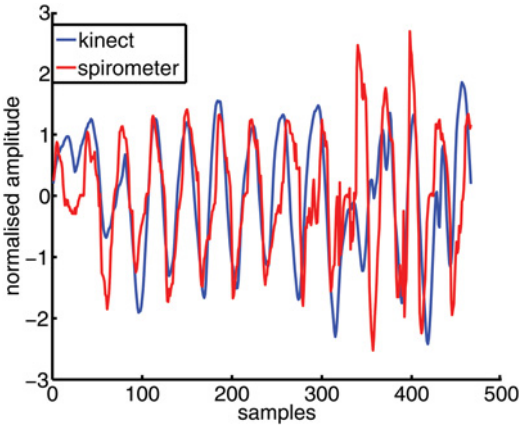

Figure 2 *Comparison between normalised signals from spirometer and camera*
The red signal represents the spirometer output, while the blue signal represents that from the camera

the value of the signal after the movement, see Fig. 3. A weighted average is calculated over a window of four mean values (calculated in step 4) to eliminate any peaks.

6. Calculation of the derivative of the weighted average: The derivative is calculated from the weighted average. In the proposed algorithm, the derivative was chosen because through its analysis it is possible to identify the maxima and the minima of the average value. The analysis of the derivative also allows elimination of irregularities in breathing.

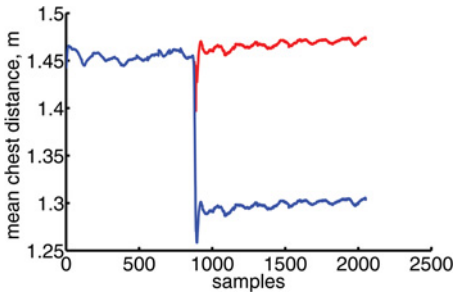

Figure 3 *Calculation of weighted average when user has moved*
Blue signal is the mean chest distance and the red signal is the same signal after the reconstruction
As it can be seen, the algorithm reconstructs the signal to calculate the respiratory rate at the instant 880, when the user moved

7. Calculation of the respiratory rate, the depth and the time of inhalation and exhalation: By identifying the local maxima and minima through the study of the derivative, it is possible to count the number of breaths during the measurement and, therefore, the number of breaths per minute. Then, it is possible to calculate the time and the depth of the breaths to understand the quality of the respiration. If the user is not breathing, the algorithm sends an alarm signal.

4. Experimental results: To evaluate the performances of the proposed respiration measurement algorithm, five sets of tests were performed. The algorithm was tested in multiple scenarios and it has proved to be robust for common domestic/home care applications. The first one is a preliminary test to choose the best sampling frequency. The second is a validation test to evaluate the goodness of the algorithm with respect to a moving user. The third, fourth and fifth are robustness tests to evaluate if the algorithm also works in different operating conditions, like a different orientation of the person, a different light condition or a different kind of clothing. In order to validate our method, a spirometer was used as gold standard. During the tests, participants needed to breathe inside a spirometer to record the respiratory course. In the meantime, the respiratory course was measured by our algorithm. The spirometer measures the amount of air inspired and expired through it, while the algorithm analyses the movement of the chest. Even if the two methods obtain the breath signal starting from two different measurements (the inspired and expired air and the chest wall motion, respectively), the maxima (and minima) of the respiratory signal must match in both cases, as it is possible to see in Fig. 2.

In these experiments, five healthy participants of both genders (three females and two males) were involved. Their age was included between 25 and 33 years old. Every participant performed three rounds of respiratory measurements, one for each test, for a total of 39 acquisitions per participant. In each round, participants could breathe as they wanted (e.g. slow/fast breathing, superficial/deep breathing, etc.). We recorded the respiratory rate with our algorithm and the spirometer, and evaluated the errors coming from their comparison. Then, for each considered condition, we calculated the mean values m_i and the standard deviations σ_i of the errors for each participant user$_i$, for $i = 1, \ldots, 5$. At the end of the tests, we calculated the mean values and the standard deviations of the previous mean values for each operating condition, M and Σ, respectively

$$M = \frac{\sum_{i=1}^{5} m_i}{5} \tag{4}$$

$$\Sigma = \sqrt{\frac{\sum_{i=1}^{5} (m_i - M)^2}{5}} \tag{5}$$

The lower M is, the better the algorithm. At the same time, the level of agreement between the respiratory rate measurements calculated by the proposed method and the spirometer was accessed using Pearson's correlation coefficient (r) and the no-correlation coefficient (p), calculated for each condition

$$r = \frac{\mathrm{cov}(X, Y)}{\sigma(X)\sigma(Y)} \tag{6}$$

$$p = 2F\left(-\left|r\sqrt{\frac{n-2}{1-r^2}}\right| | n-2\right) \tag{7}$$

where $\mathrm{cov}(X, Y)$ is the covariance between the two variables X and Y, $\sigma(X)$ and $\sigma(Y)$ are the standard deviations of the signals X and Y, respectively, $F(\cdot|\cdot)$ is the cumulative distribution function and n is the number of experiments. The Pearson's correlation coefficient

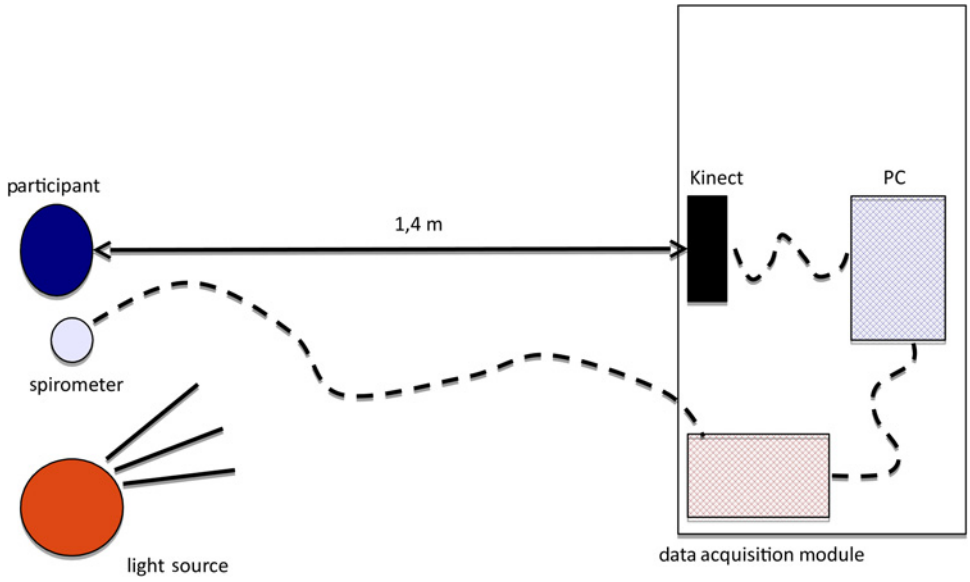

Figure 4 *Scheme of experimental environment in which tests were performed*
The user is sitting at 1.4 m from the RGB-D camera
During the acquisition, the user has to breathe inside the spirometer and he can move as he wants on the chair

measures the strength of linear association between the two variables X and Y. The coefficient is measured on a scale with no units and can assume a value from −1 to +1. If the sign of the correlation coefficient was positive, then a positive correlation exists; if the sign of the correlation coefficient was negative, then a negative correlation exists. A correlation coefficient of zero, $r = 0$, indicates no linear association between the two variables (null hypothesis).

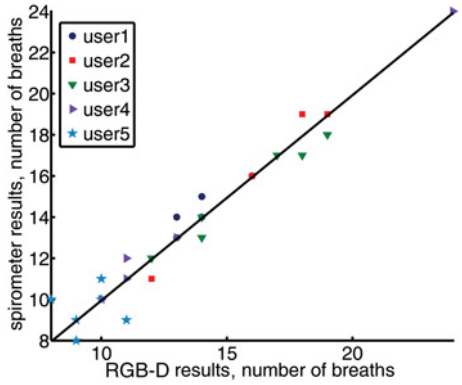

Figure 5 *Regression line and scatter plot of tests performed for moving users*

However, to be 'statistically significant', the correlation coefficient must be significantly different from zero. To reject the null hypothesis and to conclude that there is correlation between the considered variables, the no-correlation coefficient p should be lower than 0.05. The higher r is and the lower p is, then the better the algorithm performs (for more details on these indexes, refer to [19, 20]). The experiments were conducted indoors and all participants were asked to sit at a distance of 1.4 m in front of the depth camera, as detailed in Fig. 5.

4.1. Sampling rate: To choose a suitable sampling rate, a preliminary test was conducted. The respiratory rate is typically characterised by a frequency of 12–20 breaths per minute, that is, 0.2–0.33 Hz. Thus, for the chosen application, the algorithm should sample at a frequency greater than 1 Hz to perform properly. However, the sampling rate is a modifiable parameter, which could be changed to best adapt to the chosen scenario. The results obtained from sampling at a frequency of 5, 7 and 9 Hz were compared. The results are reported in Table 1. As it is possible to see, the best sampling frequency is 7 Hz, because this is the frequency which minimises the error between the measurements obtained by the algorithm and those obtained by the spirometer, and for which the correlation shows the highest value ($r = 0,\ 9802$ and $p = 10^{-10}$). A frequency of 5 Hz is too small and may cause excessive loss of data, while a frequency of

Table 1 Frequency test results

Sampling rate		user1	user2	user3	user4	user5	M	Σ	r	p
5 Hz	m_i	1	0	0	2.333	0.667	0.8	0.859	0.9133	10^{-6}
	σ_i	0	0	0	2.625	0.471				
7 Hz	m_i	0.333	0.333	0.333	0	1	0.4	0.327	0.9802	10^{-10}
	σ_i	0.471	0.471	0.471	0	0.817				
9 Hz	m_i	1.667	0	1.667	0.667	2	1.2	0.748	0.8959	10^{-6}
	σ_i	1.247	0	1.67	0.943	0.817				

m_i = error mean value, σ_i = error standard deviation. M = mean of m_i values, Σ = standard deviation of m_i values, r = correlation coefficient, p = no-correlation coefficient

doi: 10.1049/htl.2014.0063

9 Hz is too big and generates a signal with an excessive presence of noise. Note that the proposed system is a suitable monitoring system which was designed to work best with people with average breath rate. However, the chosen sampling rate can be adjusted in case the system needs to be used for monitoring people with lower or higher breath rates. In detail, the algorithm can work in a range between 2 and 24 Hz, adjustable according to the end user desire, with the sample rate and the fixed-sample average filtering designed to be independent.

4.2. Moving user and relative test results: Initially, the participants were asked to remain still in front of the camera (first scenario), then they were let free to move while sitting on the chair (second scenario). The results are reported in Table 2. As it is possible to see, in the worst case $M = 0.533$ and $r = 0.9753$, thus it is possible to conclude that the proposed algorithm can be used to measure the respiratory rate, both if the user is stationary or is moving. The regression line and the scatter plot in the algorithm tests are shown in Fig. 4.

4.3. Orientation experimental results: A typical limitation of the algorithms developed for RGB-D cameras is that they require the person to be monitored to keep a desired alignment w.r.t. the camera (e.g., frontal). In order to evaluate if the algorithm also works with a different orientation of the person, the participants were rotated 25°, such that they were no longer aligned with the camera. This value was chosen because it represents the limit of the calibration algorithm, i.e., the maximum orientation after which the algorithm of the OpenNI library fails to calibrate the user. The results are reported in Table 3. As it is possible to see, in the worst case, $M = 0.467$ and $r = 0.973$. Thus, it is experimentally proven that the orientation of the person does not affect the proposed algorithm, assuming that it does not exceed the limit imposed by the calibration algorithm.

4.4. Light experimental results: A typical limitation of the RGB-D sensor is that it is sensitive to the light conditions of the operating environment, thus different light conditions can affect the respiratory rate measurement. In order to evaluate if the results change with different light conditions, a test was conducted using three different light sources. The intensity of the lights was measured with a brightness sensor posed on the camera ($\mu V/cm^2$). The first light was the neon lamp of the room (25 $\mu V/cm^2$). The second light was a photographer spotlight (1400 $\mu V/cm^2$), positioned in front of the camera. The third light was the neon lamp of the corridor (0.7 $\mu V/cm^2$), while the neon of the room

Table 2 Algorithm test results

Type of movement		user1	user2	user3	user4	user5	M	Σ	r	p
stationary	m_i	0.333	0.333	0.333	0	1	0.4	0.327	0.9802	10^{-10}
	σ_i	0.471	0.471	0.471	0	0.817				
moving	m_i	0.333	0.333	0.667	0.333	1	0.533	0.267	0.9753	10^{-10}
	σ_i	0.471	0.471	0.471	0.471	0.817				

m_i = error mean value, σ_i = error standard deviation, M = mean of m_i values, Σ = standard deviation of m_i values, r = correlation coefficient, p = no-correlation coefficient

Table 3 Orientation test results

Orientation		user1	user2	user3	user4	user5	M	Σ	r	p
0°	m_i	0.333	0.333	0.333	0	1	0.4	0.327	0.9802	10^{-10}
	σ_i	0.471	0.471	0.471	0	0.817				
25°	m_i	0.333	1	0.333	0.333	0.333	0.467	0.267	0.9730	10^{-9}
	σ_i	0.471	0.817	0.471	0.471	0.471				

m_i = error mean value, σ_i = error standard deviation, M = mean of m_i values, Σ = standard deviation of m_i values, r = correlation coefficient, p = no-correlation coefficient

Table 4 Light test results

Light intensity		user1	user2	user3	user4	user5	M	Σ	r	p
25	m_i	0.333	0.333	0.333	0	1	0.4	0.327	0.9802	10^{-10}
	σ_i	0.471	0.471	0.471	0	0.817				
1400	m_i	0.333	0.333	0.333	1	0	0.4	0.327	0.9801	10^{-10}
	σ_i	0.471	0.471	0.471	0	0				
0.7	m_i	0	0	0.333	0.667	0.333	0.267	0.25	0.9292	10^{-7}
	σ_i	0	0	0.471	0.471	0.471				

m_i = error mean value, σ_i = error standard deviation, M = mean of m_i values, Σ = standard deviation of m_i values, r = correlation coefficient, p = no-correlation coefficient

Table 5 Clothing test results

Clothing		user1	user2	user3	user4	user5	M	Σ	r	p
sweater	m_i	0.333	0.333	0.333	0	1	0.4	0.327	0.9802	10^{-10}
	σ_i	0.471	0.471	0.471	0	0.817				
jacket	m_i	0	0.333	0.667	0.333	0.333	0.333	0.211	0.9639	10^{-9}
	σ_i	0	0.471	0.471	0.471	0.471				
t-shirt	m_i	0.333	0	0.667	0.333	0.333	0.333	0.211	0.9506	10^{-8}
	σ_i	0.471	0	0.471	0.471	0.471				

m_i = error mean value, σ_i = error standard deviation, M = mean of m_i values, Σ = standard deviation of m_i values, r = correlation coefficient, p = no-correlation coefficient

was turned off. The results are reported in Table 4. In this scenario, the worst values are $M = 0.4$ and $r = 0.9292$, proving that the algorithm works well also in different light conditions.

4.5. Clothes experimental results: To evaluate whether the algorithm is independent from the clothing, a test using three different kinds of clothing was conducted. The participant had to wear a sweater (first scenario), a jacket (second scenario) and a T-shirt (third scenario). The results are reported in Table 5. As it is possible to see, in the worst case $M = 0.4$ and $r = 0.9506$, thus it is possible to conclude that the algorithm works also with different clothes, as long as the movement of the chest is still detectable.

5. Conclusion: In this paper, a non-invasive respiratory rate measurement algorithm that uses a RGB-D camera was presented. In total, we recorded 195 rounds of respiratory measurement from five participants. The results have shown that the error between the measurements obtained by the algorithm and those obtained by the spirometer, used as a benchmark, has a maximum value of $M = 0.533$ and the correlation coefficient has a minimum value of $r = 0.9292$. Thus, it has been experimentally proven that the proposed algorithm can be used for measuring the human respiratory rate.

However, an issue was identified, that is related to the use of the OpenNI library during the calibration phase. The library needs the user to be in frontal position, with an angular orientation not exceeding 25°. When this does not happen, then two or more body joints overlap, and the algorithm does not have enough information to calibrate the target anymore. To avoid that, the algorithm should be able to identify a higher number of joints: in this way, the algorithm should be able to keep track of the person even when several joints overlap. In the future, the proposed respiratory rate measurement algorithm will be integrated with a mobile platform that implements monitoring functions to help people to live independently as long as possible in their homes.

6. Acknowledgment: The authors thank Dr. Lorenzo Scalise and his research group for their support during the experimental validation.

7 References

[1] Whyte K.F., Gugger M., *ET AL.*: 'Accuracy of respiratory inductive plethysmograph in measuring tidal volume during sleep', *J. Appl. Physiol.*, 1991, **71**, (5), pp. 1866–1871
[2] Cantineau J.P., Escourrou P., *ET AL.*: 'Accuracy of respiratory inductive plethysmography during wakefulness and sleep in patients with obstructive sleep apnea', *Chest*, 1992, **102**, (4), pp. 1145–1151
[3] BaHammam A.: 'Comparison of nasal prong pressure and thermistor measurements for detecting respiratory events during sleep', *Respiration*, 2004, **71**, (4), pp. 385–390
[4] Douglas N., Thomas S., Jan M.: 'Clinical value of polysomnography', *Lancet*, 1992, **339**, (8789), pp. 347–350
[5] Leonard P., Beattie T.F., Addison P.S., Watson J.N.: 'Standard pulse oximeters can be used to monitor respiratory rate', *Emerg. Med. J.*, 2003, **20**, pp. 524–525
[6] Nakajima K., Matsumoto Y., Tamura T.: 'Development of real-time image sequence analysis for evaluating posture change and respiratory rate of a subject in bed', *Physiol. Meas.*, 2001, **22**, (3), p. 21
[7] Wareham R., Lasenby J.J., Cameron P.D.B., Iles R.: 'Structured light plethysmography (SLP) compared to spirometry: a pilot study'. European Respiratory Society Annual Congress, Vienna, 2009
[8] Hirooki A., Kohji K.: 'Non-contact respiration monitoring method for screening sleep respiratory disturbance using slit light pattern projection'. World Congress on Medical Physics and Biomedical Engineering, Seoul, Korea, 2007, vol. 14, pp. 680–683
[9] Staderini E.: 'UWB radars in medicine', *IEEE Aerosp. Electron. Syst. Mag.*, 2002, **17**, (1), pp. 13–18
[10] Burba N., Bolas M., *ET AL.*: 'Unobtrusive measurement of subtle nonverbal behaviors with the Microsoft Kinect'. Proc. 2012 IEEE Virtual Reality (VR '12), Washington DC, WA, USA, 2012, pp. 1–4
[11] Martinez M., Stiefelhagen R.: 'Breath rate monitoring during sleep using near-IR imagery and PCA'. 21st Int. Conf. Pattern Recognition (ICPR), Tsukaba, Japan, 2012, pp. 3472–3475
[12] Yu M.C., Liou J.L., *ET AL.*: 'Noncontact respiratory measurement of volume change using depth camera'. Annual Int. Conf. IEEE Engineering in Medicine and Biology Society (EMBC), Osaka, Japan, 2012, pp. 2371–2374
[13] Yu M.C., Wu H., *ET AL.*: 'Breath and position monitoring during sleeping with a depth camera'. Int. Conf. Health Informatics, Vilamoura, Portugal, 2012, pp. 12–22
[14] Xia J., Siochi R.A.: 'A real-time respiratory motion monitoring system using KINECT: proof of concept', *Med. Phys.*, 2012, **39**, (5), pp. 2682–2685
[15] Bernal E.A., Mestha L.K., Shilla E.: 'Non-contact monitoring of respiratory function via depth sensing'. Proc. Int. Conf. Biomedical and Health Informatics, Valencia, Spain, 2014
[16] Ming-Zher P., McDuff D.J., Picard R.W.: 'Non- contact, automated cardiac pulse measurements using video imaging and blind source separation', *Opt. Express*, 2011, **18**, (10), pp. 10762–10774
[17] Mrazovac B., Bjelica M.Z., Papp I., Teslic N.: 'Smart audio/video playback control based on presence detection and user localization in home environment'. Proc. 2011 Second Eastern European Regional Conf. Engineering of Computer Based Systems (ECBS-EERC '11), Washington DC, WA, USA, 2011, pp. 44–53
[18] Khoshelham K., Elberink S.O.: 'Accuracy and resolution of Kinect depth data for indoor mapping applications', *Sensors*, 2012, **12**, (2), pp. 1437–1454
[19] Benesty J., Chen J., Huang Y., Cohen I.: 'Pearson correlation coefficient', *Noise Reduct. Speech Process.*, 2009, **2**, pp. 1–4
[20] Van Brackle L.: 'Step-by-step basic statistics using SAS: student guide', *Technometrics*, 2004, **46**, (4), pp. 494–495

doi: 10.1049/htl.2014.0063